A novel analysis of the effects of short range correlations in inclusive lepton scattering off nuclei*

Chiara Benedetta Mezzetti and Claudio Ciofi degli Atti,

Department of Physics, University of Perugia and Istituto Nazionale di Fisica Nucleare,

Sezione di Perugia, Via A.Pascoli, I-06100 Perugia, Italy

Abstract

It is shown that, if inclusive lepton scattering off nuclei at high momentum transfer ($Q^2 \gtrsim 1\,GeV^2$) is analyzed in terms of proper scaling variables, useful information on Nucleon-Nucleon short range correlations in nuclei can be obtained. The traditional approach to Y-scaling is critically analyzed and a novel approach to Y-scaling, which incorporates the effects from two- and three-nucleon correlations in nuclei, is illustrated.

arXiv:0906.5564v1 [nucl-th] 30 Jun 2009

I. INTRODUCTION

New data on inclusive quasi elastic (q.e.) electron scattering off nuclei, $A(e, e')X$, at high momentum transfer $(2.5 \lesssim Q^2 \lesssim 7.4\, GeV^2)$ are under analysis at the Thomas Jefferson National Accelerator Facility (JLab) [1]. Nowadays one of the aims of the investigation of q.e. scattering off nuclei is to obtain information on Nucleon-Nucleon (NN) short range correlations (SRC); to this end various approaches are being pursued, such as the investigation of the scaling behavior of the ratio of the inclusive cross section σ_2^A of heavy nuclei to that of ^2H and ^3He plotted versus the Bjorken scaling variable x_{Bj} [2, 3], or the analysis of cross sections in terms of Y-scaling [4]. The aim of this talk is to critically review these analyses and propose a novel approach to $A(e, e')X$ processes particularly suited to treat the effects of SRC.

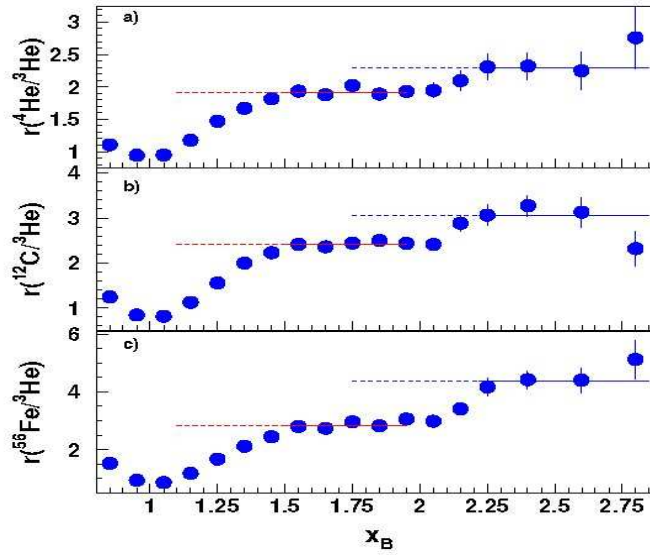# II. CROSS SECTION RATIOS: EXPERIMENTAL RESULTS

FIG. 1: The inclusive cross section ratio of ^{56}Fe, ^{12}C and ^4He to ^3He *vs.* the Bjorken scaling variable $x_B = Q^2/(2m_N\nu) \equiv x_{Bj}$. After Ref. [3].

In Fig. 1, the experimental cross section ratio $\sigma_2^A/\sigma_2^{A'} \equiv r(A/A')$ plotted versus the Bjorken scaling variable x_{Bj} is shown [3]; three distinct kinematical regions can be observed: i) the first one, at $x_{Bj} \lesssim 1.5$, is due to the contribution of mean field nucleons, and its shape is governed by the different behaviour of the magnitude of the q.e. peak for different nuclei

(higher peaks for light nuclei and lower peaks for heavy nuclei); ii) the second region, at $1.5 \lesssim x_{Bj} \lesssim 2$, exhibits a plateaux, which is interpreted as due to two-nucleon correlations (2NC); iii) the third region, at $2 \lesssim x_{Bj} \lesssim 3$, seems to show a second plateaux, which is ascribed to three-nucleon correlations (3NC). Following the original suggestion of Ref. [5], the presence of these plateaux can be viewed as evidence that two- and three-nucleon correlations in complex nuclei and in ^3He differ only by a scale factor. It should however be pointed out that no direct calculations of the cross section ratio shown in Fig. 1 have been performed so far. These calculations would represent a relevant contribution towards the solution of the longstanding problem concerning the role played by SRC in nuclei. Here, preliminary results of the calculation of the ratio $r(A/A')$ will be given. In order to illustrate the basic ideas of our approach [6], some general concepts of Y-scaling have to be recalled.

III.   INCLUSIVE LEPTON SCATTERING AND Y-SCALING

In PWIA, the inclusive q.e. cross section can be written as follows [7]

$$\sigma_2^A(q,\nu) \equiv \frac{d^2\sigma(q,\nu)}{d\Omega_2\,d\nu} = F^A(q,\nu)\,K(q,\nu)\,[Z\sigma_{ep} + N\sigma_{en}] \tag{1}$$

where

$$F^A(q,\nu) = 2\pi \int_{E_{min}}^{E_{max}(q,\nu)} dE \int_{k_{min}(q,\nu,E)}^{k_{max}(q,\nu,E)} k\,dk\,P^A(k,E) \tag{2}$$

is the nuclear structure function, $\mathbf{q} = \mathbf{k}_1 - \mathbf{k}_2$ ($|\mathbf{q}| = q$) and $\nu = \epsilon_1 - \epsilon_2$ are the three-momentum and energy transfers, σ_{eN} is the elastic electron cross section off a moving off-shell nucleon with momentum $k \equiv |\mathbf{k}|$ and removal energy E, $K(q,\nu)$ is a kinematical factor, and, eventually, $P^A(k,E)$ is the spectral function. For ease of presentation, we will consider high values of the momentum transfer, such that $E_{max}(q,\nu)$ and $k_{max}(q,\nu,E)$ become very large, in which case, owing to the rapid falloff of $P^A(k,E)$ with k and E, the replacement $E_{max} = k_{max} = +\infty$ is justified. Without any loss of generality, we can substitute the energy transfer ν with a generic "scaling variable" $Y = Y(q,\nu)$; in this case, the "scaling function" (2) can be written as follows [7]

$$F^A(q,Y) = f^A(Y) - B^A(q,Y) \tag{3}$$

where the first term

$$f^A(Y) = 2\pi \int_{|Y|}^{\infty} k\,dk\,n^A(k) \tag{4}$$

3

is the longitudinal momentum distribution, and the second one

$$B^A(q, Y) = 2\pi \int_{E_{min}}^{\infty} dE \int_{|Y|}^{k_{min}(q,Y,E)} k \, dk \, P_1^A(k, E) \qquad (5)$$

is the so called "binding correction". The longitudinal momentum distribution depends
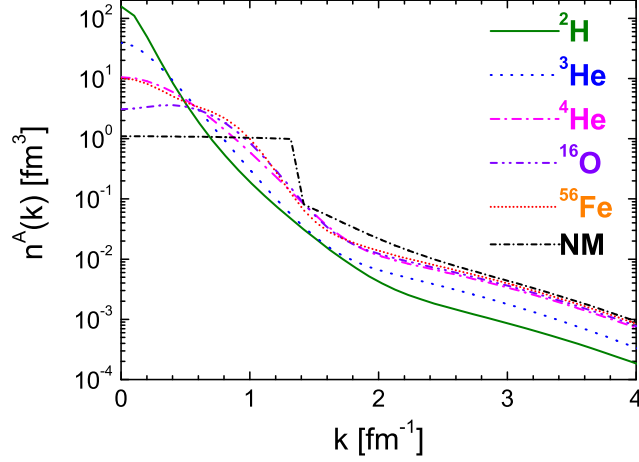

FIG. 2: The nucleon momentum distributions $n^A(k)$ for nuclei ranging from ^2H to NM. It can be seen that, at high values of the momentum k, $n^A(k)$ can be considered as a rescaled version of the momentum distributions of ^2H. After Ref. [9].

only upon the nucleon momentum distributions $n^A(k) = \int P^A(k, E) \, dE$, which, as is well known [8] and illustrated in Fig. 2, at high values of the momentum k scale with A according to $n^A(k) \simeq C^A \, n^D(k)$; the binding correction $B^A(q, Y)$, on the contrary, depends upon the correlated part of the spectral function $P_1^A(k, E)$ (as is well known, $P^A(k, E) = P_0^A(k, E) + P_1^A(k, E)$, where $P_0^A(k, E)$ is the (trivial) shell-model part and $P_1^A(k, E)$ is the (interesting) part generated by NN correlations [10]). In the Deuteron case, one has $E = E_{min} = 2.22 \, MeV$, $k_{min}(q, Y, E_{min}) = |Y|$, $B^D(q, Y) = 0$ and $F^D(q, Y) = f^D(Y)$, from which the nucleon momentum distributions can be obtained by the relation $n^A(k) = -[df^A(Y)/dY]/[2\pi Y]$; in general, however, $B^A(q, Y) \neq 0$ and $F^A(q, Y) \neq f^A(Y)$ and the momentum distributions cannot be obtained. The central idea of our approach [6], is that the contribution arising from the binding correction could be minimized by a proper choice of the scaling variable Y, such that $k_{min}(q, Y, E) \simeq |Y|$, with the resulting cross section (1) depending only upon the nucleon momentum distributions, obtaining, by this way, a direct access to high momentum components generated by SRC.

4

It is clear that the outlined picture can in principle be modified by the effects of the final state interactions (FSI); this important point will be discussed later on.

A. Traditional approach to Y-scaling: the mean field scaling variable

The traditional scaling variable, usually denoted by small y, $Y \equiv y$, is obtained by placing $k = |y|$, $\cos \alpha = (\mathbf{k} \cdot \mathbf{q}/kq) = 1$ and $E^*_{A-1} = 0$ in the energy conservation law given by

$$\nu + M_A = \sqrt{(M_{A-1} + E^*_{A-1})^2 + \mathbf{k}^2} + \sqrt{m_N^2 + (\mathbf{k} + \mathbf{q})^2} \tag{6}$$

where E^*_{A-1} is the intrinsic excitation energy of the $(A-1)$-nucleon system and the other notations are self explained. In such an approach, y represents the minimum longitudinal momentum of a nucleon having the minimum value of the removal energy $E = E_{min} + E^*_{A-1} = E_{min} = m_N + M_{A-1} - M_A$. In the asymptotic limit, $(q \to \infty)$, one has $k^\infty_{min}(q, y) =$

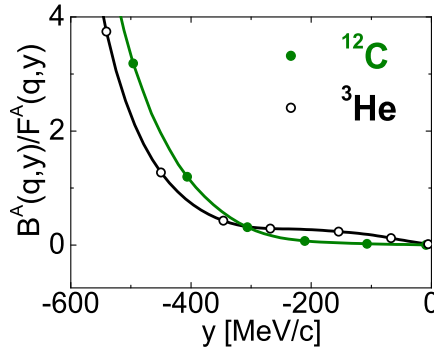FIG. 3: The ratio of the binding correction $B^A(q, y)$ (Eq. (5)) to the scaling function $F^A(q, y)$ (Eq. (2)) for ^3He (open dots) and ^{12}C (full dots), calculated using the scaling variable y. After Ref. [6].

$|y - (E - E_{min})|$ [7], so that, when $E = E_{min}$, $k^\infty_{min}(q, y) = |y|$ and $B^A(q, y) = 0$; this occurs only when $A = 2$, whereas in the general case, $A > 2$, the excitation energy E^*_{A-1} of the residual system is different from zero, leading to $B^A(q, y) > 0$. The binding correction plays indeed a relevant role in the traditional approach to Y-scaling. To illustrate this, the ratio $B^A(q, y)/F^A(q, y)$ is shown in Fig. 3; it can be seen that at high (negative) values of y, the effects from binding are very large. Moreover, the experimental scaling function $F^A_{exp}(q, y) = \sigma_{exp}/[K(q, y) (Z\sigma_{ep} + N\sigma_{en})]$ plotted versus the scaling variable y confirms, as shown in Fig. 4, that the scaling function strongly differs from the longitudinal momentum
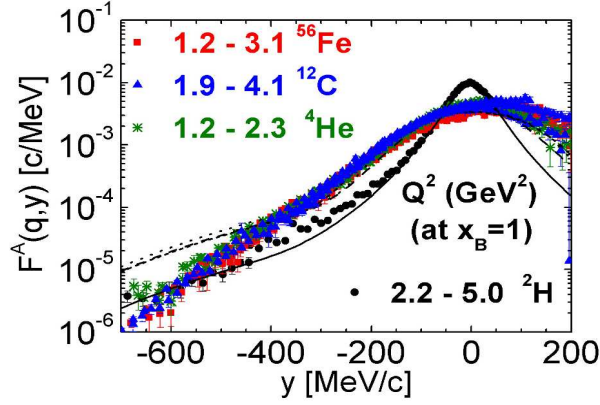
FIG. 4: The experimental scaling function $F_{exp}^A(q,y)$ of ^4He, ^{12}C, and ^{56}Fe obtained from the experimental data of Refs. [11, 12]. The longitudinal momentum distributions (Eq. (4)) of ^2H (full line), ^4He (long-dashed), ^{12}C (dashed) and ^{56}Fe (dotted) are also shown. After Ref. [6].

distribution, and therefore does not exhibits any proportionality to the Deuteron scaling function $f^D(y)$.

B. A novel approach to Y-scaling: the scaling variable embedding two-nucleon correlations

2NC are defined as those nucleon configurations shown in Fig. 5 [2]: momentum conservation in the ground state of the target nucleus ($\sum_1^A \mathbf{k}_i = 0$) is almost entirely exhausted by two correlated nucleons with high momenta, the $(A-2)$-nucleon system acting mainly as a spectator, moving with very low momentum. The intrinsic excitation energy of the

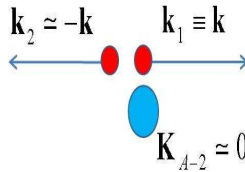
FIG. 5: 2NC correlations in a nucleus A: the high momentum $\mathbf{k}_1 \equiv \mathbf{k}$ of nucleon "1" is almost completely balanced by the momentum $\mathbf{k}_2 \simeq -\mathbf{k}$ of the partner nucleon "2", whereas the residual system moves with low momentum $\mathbf{K}_{A-2}$. Momentum conservation is $\sum_1^A \mathbf{k}_i = \mathbf{k}_1 + \mathbf{k}_2 + \mathbf{K}_{A-2} = 0$.

$(A-1)$-nucleon system is in this case

$$E_{A-1}^* = \frac{(A-2)}{(A-1)} \frac{(\mathbf{k}_2 - \mathbf{K}_{A-2})^2}{2m_N} \tag{7}$$

6

which becomes

$$E_{A-1}^* = \frac{(A-2)}{(A-1)} \frac{k^2}{2m_N} \tag{8}$$

in the naive 2NC model, i.e. the model based upon the assumption $\mathbf{K}_{A-2} = 0$. Since high excitation states of the final $(A-1)$-nucleon system are generated by SRC in the ground state of the target nucleus, the traditional (mean field) scaling variable y does not incorporate, by definition, SRC effects, for it is obtained by placing $E_{A-1}^* = 0$ in the energy conservation law (6). Motivated by this observation, in Ref. [4], a new scaling variable $Y \equiv y_{CW} \equiv y_2$ has been introduced by setting in Eq. (6) $k = |y_2|$, $\cos \alpha = (\mathbf{k} \cdot \mathbf{q}/kq) = 1$ and $E_{A-1}^* = < E_{A-1}^*(k) >_{2NC}$. By this way, y_2 properly includes the momentum dependence of the average excitation energy of the $(A-1)$-nucleon system generated by SRC. The approach of Ref. [4] has been further improved in Ref. [6], obtaining a scaling variable y_2 which, through the k dependence of $< E_{A-1}^*(k) >_{2NC}$, interpolates between the correlations and the mean field regions of the q.e. cross section. The relevant feature of y_2 is that it leads to $k_{min}(q, y_2, E) \simeq |y_2|$ and therefore to a minor role of the binding correction; this is indeed demonstrated in Fig. 6, which clearly shows that $B^A(q, y_2)$ vanishes in the whole region of y_2 considered. One can therefore conclude that, using the new scaling variable, one obtains $F^A(q, y_2) \sim f^A(y_2) \sim C^A f^D(y_2)$.
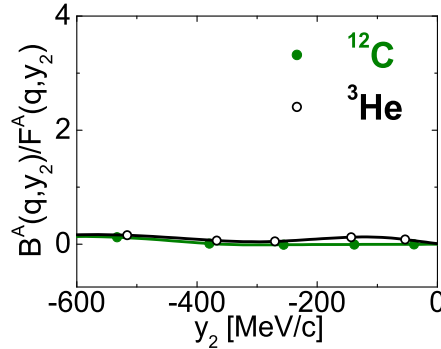

FIG. 6: The same as in Fig. 3, obtained using in Eqs. (2) and (5) the scaling variable $y_2 \equiv y_{CW}$. After Ref. [6].

The scaling function $F^A(q, y_2)$ obtained from available experimental data on ^4He, ^{12}C and ^{56}Fe is plotted in Fig. 7 versus the scaling variable y_2; it can be seen that at high values of $|y_2|$, the relation $F^A(q, y_2) \sim f^A(y_2) \sim C^A f^D(y_2)$ is indeed experimentally confirmed.
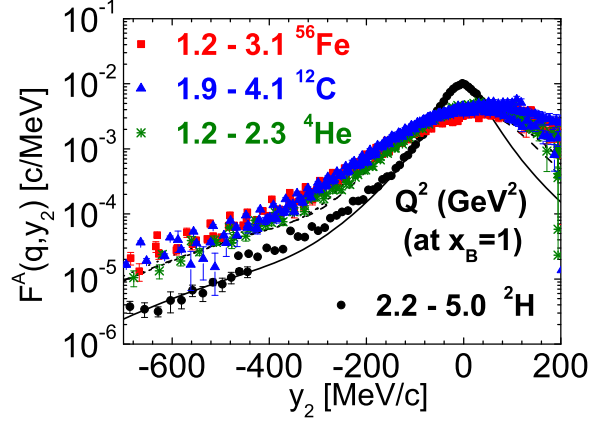
FIG. 7: The same as in Fig. 4 *vs.* the scaling variable $y_2 \equiv y_{CW}$. After Ref. [6].

In order to analyze more quantitatively the scaling behavior of $F^A(q, y_2)$, the latter has been plotted versus Q^2, at fixed values of y_2. The result is shown in Fig. 8, together with
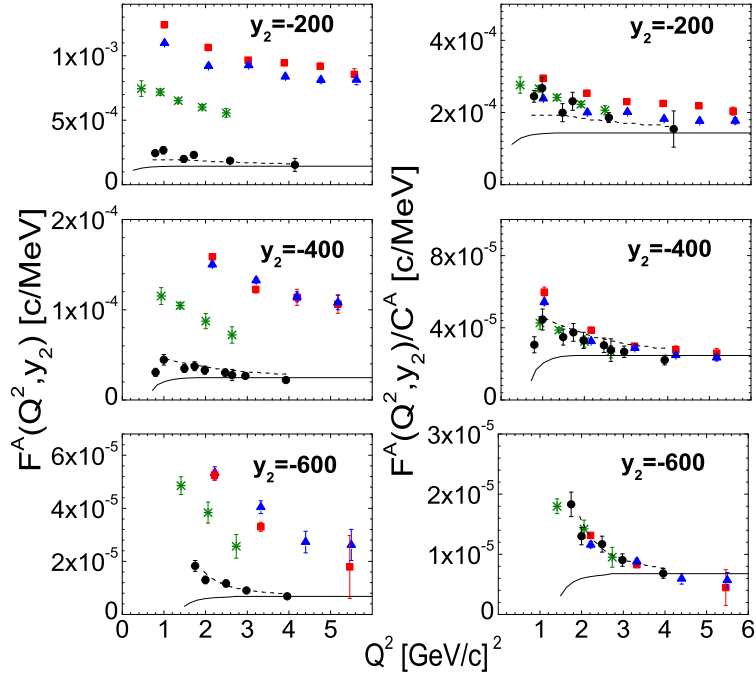

FIG. 8: *Left panel*: the scaling function $F^A(Q^2, y_2)$ *vs.* Q^2, at fixed values of $y_2 \equiv y_{CW}$. *Right panel*: the same data divided by the constants $C^4 = 2.7$, $C^{12} = 4.0$ and $C^{56} = 4.6$, respectively for ^4He, ^{12}C and ^{56}Fe. The theoretical curves represent the longitudinal momentum of the Deuteron, calculated (AV18 interaction) in PWIA (full line) and including FSI (dashed line) effects. After Ref. [6].

the theoretical scaling function for $A = 2$, calculated in PWIA (solid line), and taking FSI into account (dashed line). It can be seen (left panel) that, due to FSI effects, scaling is violated and approached from the top, and not from the bottom, as predicted by the PWIA. However, the violation of scaling seems to exhibit a Q^2 dependence which is very similar in Deuteron and in complex nuclei. This is illustrated in more details in the right panel of the figure, which shows $F^A(Q^2, y_2)$ divided by a constant C^A, chosen so as to obtain the Deuteron scaling function $F^D(Q^2, y_2)$. It clearly appears that the scaling function of heavy and light nuclei scales to the Deuteron scaling function; moreover the values obtained for C^A turn out to be in agreement with the ones predicted in Ref. [2]; it is also important to stress that, although FSI are very relevant, they appear to be similar in Deuteron and in a nucleus A, which is evidence that, in the SRC region, FSI are mainly restricted to the correlated pair.

C.   A novel approach to Y-scaling: the scaling variable embedding three-nucleon correlations

Let us now consider three-nucleon correlations. These correspond to those three-nucleon configurations when the high momentum $\mathbf{k}_1 \equiv \mathbf{k}$ of nucleon "1" is almost entirely balanced by the momenta $\mathbf{k}_2$ and $\mathbf{k}_3$ of nucleons "2" and "3". The excitation energy of the $(A-1)$-nucleon system is given in this case by

$$E^*_{A-1} = \frac{(\mathbf{k}_2 - \mathbf{k}_3)^2}{m_N} + \frac{A-3}{A-1} \frac{[(\mathbf{k}_2 + \mathbf{k}_3) - 2\mathbf{K}_{A-3}]^2}{4m_N} \tag{9}$$

Eq. (9) shows that, whereas 2NC are directly linked to high values of excitation energies $E^*_{A-1} \simeq (A-2)\, k^2/2m_N(A-1)$, high momentum components due to 3NC may lead both to low and to high values of E^*_{A-1}, as shown in the examples of Figs. 9(a) and 9(b), respectively. In the configuration of Fig. 9(a), the momentum $\mathbf{k}_1 \equiv \mathbf{k}$ of nucleon "1" is almost entirely balanced by nucleons "2" and "3", with momenta $\mathbf{k}_2 \simeq \mathbf{k}_3 \simeq -\mathbf{k}/2$, and one has

$$E^*_{A-1} = \frac{A-3}{A-1} \frac{k^2}{4m_N} \tag{10}$$

In the configuration of Fig. 9(b), $k_2 = k_3 = -|\mathbf{k}|\cos(\theta/2)/2$, with $\cos\theta = -(\mathbf{k}_2 \cdot \mathbf{k}_3)/(k_2 k_3)$, and E^*_{A-1} could be very large. Let us investigate the presence and relevance of 3NC configurations in the spectral function of the 3-nucleon system for which the Schroedinger equation
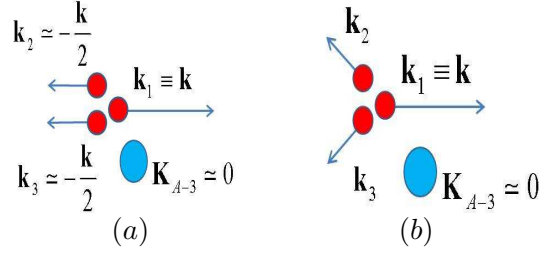
9

FIG. 9: Two types of 3NC configurations which are present in the spectral function of a nucleus A; they correspond to: (a) high momentum k and low removal energy E, and (b) to high momentum k and high removal energy E.

has been solved exactly. When $A = 3$, 3NC of the type shown in Fig. 9(a) lead to $E_2^* = 0$. In Fig. 10, the realistic spectral function of ^3He obtained [13] using the Pisa wave function [14] corresponding to the AV18 interaction [15] (full squares), is compared with the predictions of the 2NC model (solid line) [9] and with a model which includes also 3NC of the type depicted in Fig. 9(a) (dashed line) [16]. It can be observed that 2NC reproduce the exact spectral function in a wide range of removal energies ($50 \lesssim E \lesssim 200\,MeV$), but fail at very low and very high values of E, where the effects from 3NC are expected to provide an appreciable contribution. It is clear from Fig. 10 that 3NC of the type shown in Fig. 9(b)
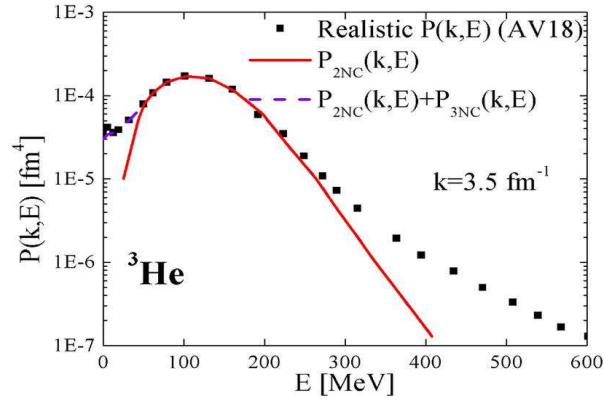

FIG. 10: The spectral function of ^3He vs. the removal energy E, at $k = 3.5\,fm^{-1}$ [13]. The realistic spectral function corresponding to the Pisa wave function (squares) is compared with the 2NC model of Ref. [9] (full line) and with a model which includes also 3NC (dashed line) of the type depicted in Fig. 9(a) [16].

can hardly be present in the spectral function at $k < 3.5 fm^{-1}$ and $E \leq 300\,MeV$, so that

it is legitimate to ask ourselves whether these 3NC can show up in available experimental data. To answer this question, let us now consider the maximum value of the removal energy achieved in the experiments, i.e. the upper limit of integration in Eq. (2),

$$E_{max}(q, \nu) = \sqrt{(\nu + M_A)^2 - q^2} \qquad (11)$$

In Fig. 11, we show $E_{max}(q, \nu)$ plotted versus the Bjorken scaling variable in the region $1 \leq x_{Bj} \leq 3$ in correspondence of a set of values of ν and q typical of available experimental data on ^3He. It can be seen from Figs. 10 and 11 that in the region $2 \leq x_{Bj} \leq 3$ only 3NC configurations of the type shown in Fig. 9(a) can contribute to present $A(e, e')X$ kinematics; for this reason we will consider, for the time being, only this type of 3NC .
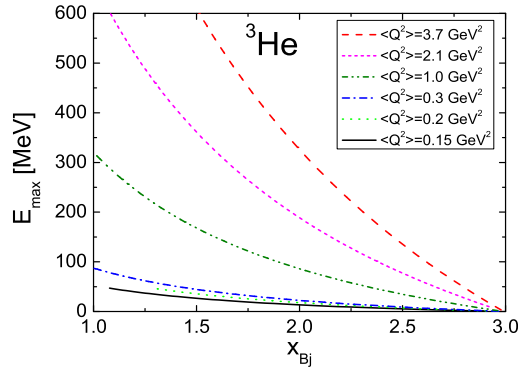

FIG. 11: The maximum value of the removal energy E_{max} (Eq. (11)) available in inclusive q.e. scattering off ^3He plotted *vs.* x_{Bj} at increasing values of Q^2, shown in the inset.

The scaling variables y and y_2 have been obtained by placing different values of E^*_{A-1} in Eq. (6), namely $E^*_{A-1} = 0$ and $E^*_{A-1} = < E^*_{A-1}(k) >_{2NC}$, respectively. Following the same procedure, we have derived the scaling variable embedding 3NC, $Y \equiv y_3$, by placing in Eq. (6) $E^*_{A-1} = < E^*_{A-1}(k) >_{3NC}$, with $< E^*_{A-1}(k) >_{3NC}$ calculated within the 3NC configuration 9(a), which corresponds to high values of k and small values of E. The explicit expression for y_3 will be given elsewhere [16]. Here we show in Fig. 12, in the case of ^{56}Fe, the values of y, y_2 and y_3 plotted versus x_{Bj}. It can be seen that, because of the different values of E^*_{A-1} used in Eq. (6), different limits of existence of the three scaling variables are obtained: y describes the mean field configuration and is defined in the whole range of $x_{Bj} \leq A$; y_2 represents 2NC in heavy nuclei resembling the ones acting in Deuteron and is defined only
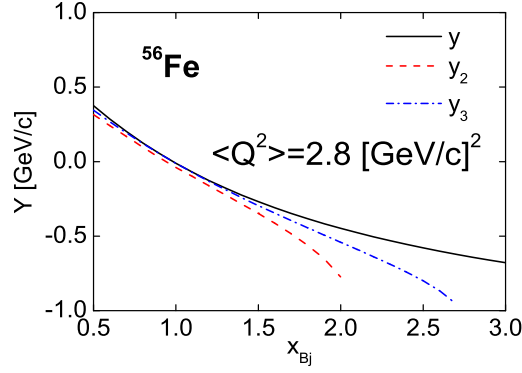
FIG. 12: The scaling variables y, y_2 and y_3 *vs.* x_{Bj} for $A = 56$.

for $x_{Bj} \leq 2$; y_3, eventually, describes 3NC as in ^3He, and is defined only for values of x_{Bj} up to 3.

IV. CROSS SECTION RATIO: PRELIMINARY RESULTS

As mentioned in previous sections, our novel approach to inclusive lepton scattering off nuclei is based upon the introduction of proper scaling variables that effectively include the energy E^*_{A-1} of the residual system and allow one to describe the $A(e, e')X$ cross section only in terms of nucleon momentum distributions generated by 2N and 3N SRC, i.e.

$$
\frac{d^2\sigma}{d\Omega_2 \, d\nu} \propto \int_{E_{min}}^{E_{max}(q,\nu,E)} dE \int_{k_{min}(q,\nu,E)}^{k_{max}(q,\nu,E)} kdk \, P^A(k, E)
$$
$$
\simeq \int_{|y|}^{\infty} n_0^A(k) \, kdk + \int_{|y_2|}^{\infty} n_2^A(k) \, kdk + \int_{|y_3|}^{\infty} n_3^A(k) \, kdk
$$

(12)

where $n_0^A(k)$ is the component of the nucleon momentum distribution generated by the mean field,

$$
n_2^A(k) = \int dk_{CM} \, n_{rel}(\mathbf{k} + \mathbf{k}_{CM}) \, n_{CM}^{soft}(\mathbf{k}_{CM})
$$

(13)

is the one due to 2NC and, eventually,

$$
n_3^A(k) = \int dk_{CM} \, n_{rel}(\mathbf{k} + \mathbf{k}_{CM}) \, n_{CM}^{hard}(\mathbf{k}_{CM})
$$

(14)

is the one due to 3NC; here, n_{CM}^{soft} and n_{CM}^{hard} include only "soft" and "hard" momentum components, respectively. Within such an approach, the cross section ratio $r(A/A')$ reduces
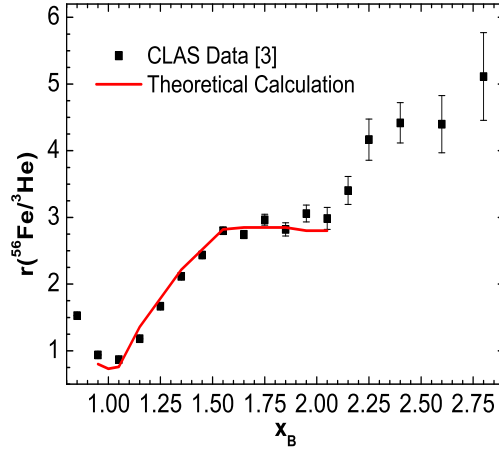
12

FIG. 13: The experimental cross section ratio shown in Fig. 1 compared with our preliminary theoretical results.

to the scaling function ratio of nuclei A and A'. Our preliminary calculations of the scaling function ratio, performed for $A = 56$, show in PWIA a good agreement with CLAS data only for $1.5 \lesssim x_{Bj} \lesssim 2$, i.e. in the region of 2NC; on the contrary, at $x_{Bj} \lesssim 1.5$, the PWIA does not lead to satisfactory results. This fact agrees with the results already shown in Fig. 8: in the region of 2NC the data of heavy nuclei scale to the Deuteron ones, and thus FSI effects vanish in the ratio $r(A/A')$, leading to the first plateaux; in the kinematical region at $x_{Bj} \lesssim 1.5$, on the opposite, the ratio exhibits a strong sensitivity upon the A-dependent FSI of the knocked nucleon with the residual system. Including explicitly these FSI effects in the mean field contribution, we obtained the preliminary results shown in Fig. 13. Calculations of 3NC effects in the region $2 \lesssim x_{Bj} \lesssim 3$ are in progress and will reported elsewhere [16].

V.   CONCLUSIONS

To sum up, the following remarks are in order:

- the experimental scaling function in the 2NC region scales to the Deuteron scaling function and exhibits A-independent FSI effects, mostly due to the FSI in the correlated pair;

- proper scaling variables have been introduced which effectively include the excitation

13

energy E_{A-1}^* of the residual system in different ways and allow one to describe the $A(e, e')X$ cross section in terms of the corresponding momentum distributions generated by 2NC and 3NC;

- the experimental ratio $r(^{56}Fe/^3He)$ in the 2NC region has been successfully reproduced.

Calculations including the 3NC configurations of the type shown in Fig. 9(b), which are necessary in order to extend our comparison with the CLAS experimental data to the region $2 \lesssim x_{Bj} \lesssim 3$, are in progress and the explicit introduction of FSI within the correlated pair is being considered [16].

---

[1] N. Fomin, arXiv:0808.2625; D. Day, in *Sixth International Conference on Perspectives in Hadronic Physics*, S. Boffi, C. Ciofi degli Atti, M. Giannini, D. Treleani Eds., AIP Conf. Proc. (2008) Vol. 1056, p. 315

[2] L.L. Frankfurt, M.I. Strikman, D.B. Day and M. Sargsian, *Phys. Rev.* **C 48**, 2451 (1993).

[3] K.S. Egyian *et al Phys. Rev. Lett.* **96**: 082501 (2006).

[4] C. Ciofi degli Atti and G. B. West, *Phys. Lett.* **B 458**, 447 (1999).

[5] L.L. Frankfurt, M.I. Strikman, *Phys. Rep.* **5**, 235 (1988).

[6] C. Ciofi degli Atti and C.B. Mezzetti, *Phys. Rev.* **C 79**, 051302(R) (2009).

[7] C. Ciofi degli Atti, E. Pace and G. Salmè, *Phys. Rev.* **C 36**, 1208 (1987); **C43**, 1155 (1991).

[8] S. C. Pieper, R. B. Wiringa and V. R. Pandharipande, *Phys. Rev.* **C 46**, 1741 (1992)

[9] C. Ciofi degli Atti and S. Simula, *Phys. Rev.* **C 53**, 1689 (1996).

[10] C. Ciofi degli Atti and S. Liuti, *Phys. Lett.* **B 225**, 215 (1984).

[11] W. Schutz *et al, Phys. Rev. Lett.* **38**, 259 (1977); *ibid.* **49**, 1139 (1982).

[12] J. Arrington, *Ph.D. Thesis*, California Institute of Technology, (2006); arXiv:nucl-ex/0608013.

[13] C. Ciofi degli Atti and L.P. Kaptari, *Phys. Rev.* **C 66**, 044004 (2002)

[14] A. Kievsky, S. Rosati and M. Viviani, *Nucl. Phys.* **A551**, 241 (1993).

[15] R. B. Wiringa, V. G. J. Stoks and R. Schiavilla, *Phys. Rev.* C **51**, 38 (1995).

[16] C.Ciofi degli Atti, C.B. Mezzetti, to be published.